# Theoretical studies on cerium nickel aluminides: polar intermetallics with heavy fermion behavior

Delphine Gout,[*] Evan Benbow, Olivier Gourdon, and Gordon J. Miller

*Department of Chemistry, Iowa State University, Gilman Hall, Ames, IA 50011-3111, USA*

**Abstract**

The electronic structures of $Ce_4Ni_6Al_{23}$, $CeNiAl_4$, $CeNi_2Al_5$, $CeNiAl$ and $CeNi_4Al$ have been calculated using the TB-LMTO-ASA (tight-binding, linear muffin-tin orbital, atomic-spheres approximation) approach to probe relationships between chemical bonding and physical properties in this series of intermetallic compounds. Analysis from crystal orbital Hamilton populations (COHP) reveal that the Al-rich compounds may be considered as "polar intermetallic" because the Fermi level coincides to the separation of bonding and antibonding states of the Ni–Al framework. On the other hand, although the densities of states (DOS) of $CeNiAl$ suggest "polar intermetallic" behavior, the bonding is more complex. Finally, the Ni-rich example, $CeNi_4Al$, has significant Ni-$3d$ character at the Fermi level. The results of these calculations are also discussed in connection with heavy fermion or possible valence fluctuation behavior observed for some of these intermetallic compounds: those showing exceptional properties also exhibit significant "lattice covalency" between Ce and the Ni–Al nets.
© 2003 Elsevier Inc. All rights reserved.

*Keywords:* Intermetallic compounds; Aluminum; Cerium; Nickel; Ab initio band structure calculations; Heavy-fermion system; Polar intermetallic

## 1. Introduction

Strong electron–electron correlation is one of the central issues of current condensed matter physics. This phenomenon impacts several classes of compounds such as high-temperature superconductors, colossal magnetoresistant materials, intermediate/mixed valence compounds, and heavy-fermion materials. Heavy-fermion materials are unconventional because the conduction electrons are strongly coupled with the magnetic moments of the valence $f$-electrons [1]. At room temperature these materials behave as normal metals in which the $f$-electrons interact weakly with conductions electrons and display local-moment magnetic properties, but at low temperatures ($T < 20$ K), unique and interesting properties appear. For example, the linear coefficient of the specific heat, $\gamma_0 = C/T$, is extremely high compared with that of conventional metals ($\gamma_0$ typically exceeds 400 mJ/mol K$^2$). This high $\gamma_0$ value is the result of hybridization between conduction electrons and $f$-electrons. However, such strong

hybridization could also give rise to valence fluctuations, which may also be at the origin of low-temperature magnetic susceptibility and resistance behavior similar to heavy-fermion materials. Such valence fluctuations are observed in $CeSn_3$ [2], which involves mixed $Ce^{3+}/Ce^{4+}$ valence states at low temperature (under 100 K). Indeed, explanations of such physical properties at low temperature remain controversial.

In the past few decades, many cerium compounds showing heavy-fermion behavior have been investigated. In the ternary Ce–Ni–Al system, Zarechnyuk et al. [3] crystallographically confirmed four different ternary intermetallic compounds. Among these compounds, $CeNiAl_4$ and $CeNi_2Al_5$ have received more attention with numerous measurements of their temperature-dependent electrical resistivity, magnetization and specific heat [4–11]. Recently, we synthesized a new compound in this system, $Ce_4Ni_6Al_{23}$ [12], which shows a new structure type and physical properties similar to $CeNiAl_4$ and $CeNi_2Al_5$. Compounds of this general type, i.e., active metal-late transition metal-post transition metal with low concentrations of the active metal often behave as so-called "polar intermetallic" compounds [13,14]. For such compounds, the active metal

[*]Corresponding author. Fax: +515-294-0105.
*E-mail address:* gmiller@iastate.edu (D. Gout).

donates its valence electrons to the electronegative metals, which, in turn, adopt a structure that optimizes its metal–metal bonding as determined by overlap populations between the electronegative metals.

The aim of this work is using TB-LMTO-ASA band structure calculations to explore chemical parameters consistent with heavy-fermion behavior or valence fluctuations as well as metal–metal bonding in the Ce–Ni–Al system. Indeed, electronic structure calculations have been useful for other heavy-fermion cases such as $CeRh_2Si_2$, $CeIn_3$, $CePd_2Si_2$, and $CeRhIn_5$ [15]. To understand the influence of the local environment of the Ce and Ni atoms and metal–metal bonding in the Ni–Al framework on the physical and chemical properties, we have carried out band structure calculations on the series $Ce_4Ni_6Al_{23}$, $CeNiAl_4$, $CeNi_2Al_5$, CeNiAl and $CeNi_4Al$.

## 2. Structures and physical properties

A partial phase diagram of the Ce–Ni–Al system at 1073 K, illustrated in Fig. 1, shows five compounds separated into three different regions: $CeNiAl_4$ ($YNiAl_4$-type), $Ce_4Ni_6Al_{23}$ and $CeNi_2Al_5$ ($PrNi_2Al_5$-type) in the Al-rich portion; CeNiAl ($Fe_2P$-type); and $CeNi_4Al$ ($CaCu_5$-type) in the Ni-rich region. Fig. 2 shows the different atomic arrangements observed in these five ternary compounds with the Ni–Al network emphasized. Among the unit cells of each compound, shown at the top of Fig. 2, the orthorhombic unit cell
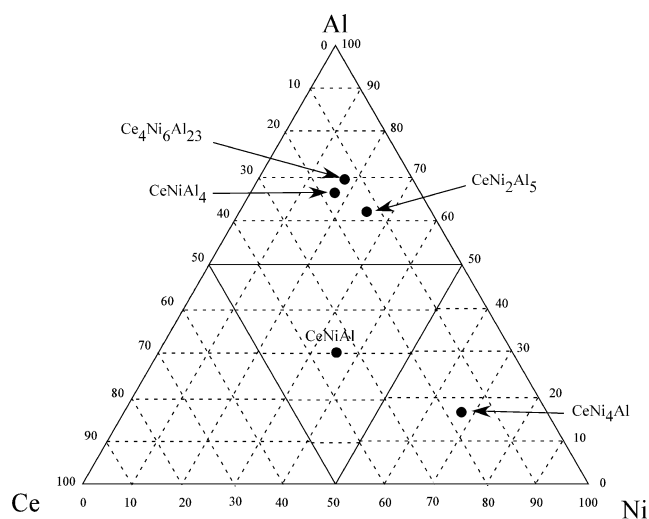


Figure 1

Fig. 1. Partial phase diagram of the Ce–Ni–Al system at 1073 K. Five compounds separated into three different regions are represented: $CeNiAl_4$ ($YNiAl_4$-type), $Ce_4Ni_6Al_{23}$ and $CeNi_2Al_5$ ($PrNi_2Al_5$-type) in the Al-rich portion; CeNiAl ($Fe_2P$-type); and $CeNi_4Al$ ($CaCu_5$-type) in the Ni-rich region.

of $CeNi_2Al_5$ is more or less observed in all cases, and is highlighted by dashed lines. The Ce environments ($d < 3.8$ Å) are rather similar for $CeNiAl_4$ (13 Al and 4 Ni; site symmetry $mm2$), $Ce_4Ni_6Al_{23}$ (13 Al and 2 Ni; site symmetry $m$), $CeNi_2Al_5$ (14 Al and 4 Ni; site symmetry $mmm$), and even $CeNi_4Al$ (4 Al and 14 Ni; site symmetry $6/mmm$), which have Ce compositions less than 17 atomic percent. With 33 at % Ce in CeNiAl, a different Ce environment is observed with other Ce atoms in its surrounding (3 Ce, 5 Ni and 6 Al). The Ni environments ($d < 3.5$ Å), also shown in Fig. 2, are tricapped trigonal prisms with one exception in $CeNi_4Al$. For $CeNiAl_4$ and $CeNi_2Al_5$ a similar trigonal prismatic site of 4 Al and 2 Ce atoms capped by three Al atoms is observed. In $Ce_4Ni_6Al_{23}$ the three crystallographically independent Ni positions show some noticeable differences [12]: one is coordinated as in $CeNiAl_4$; a second by nine Al atoms, while the third site is surrounded by 8 Al atoms and 2 Ce atoms. For CeNiAl, two distinct crystallographically independent Ni positions are refined. Both environments are tricapped trigonal prisms: one is a prism of Al tricapped by Ce; the other, a prism of Ce tricapped by Al. A common point between CeNiAl and the compounds in the Al-rich region are Ni–Ni distances exceeding 4 Å, which prohibit significant Ni–Ni interactions. Finally, in $CeNi_4Al$ one set of Ni atoms center trigonal prisms of 4 other Ni atoms and 2 Al atoms that are capped by three Ce sites. The other site is surrounded by a distorted cuboctahedron of 4 Ce, 6.67 Ni and 1.33 Al atoms. Neutron diffraction studies by Moze and Buschow [16] demonstrated that Al atoms fractionally (and randomly) occupy this second site. Nevertheless, the high concentration of Ni in this compound leads to significant Ni–Ni interactions. The major interatomic distances in all these compounds are listed in the literature [4–11].

If we focus on interatomic distances less than 3.1 Å, then there is also a network description to many of these structures. $CeNiAl_4$ and $CeNi_2Al_5$ contain puckered, nearly close packed $[NiAl_2]$ sheets with different spacers: in $CeNiAl_4$, these atomic layers are interspersed with undulating $[Al_2]$ sheets; whereas in $CeNi_2Al_5$, these $[NiAl_2]$ layers are connected by single Al atoms, whose coordination environment is close to $bcc$. $Ce_4Ni_6Al_{23}$ contains aspects of both these features. CeNiAl, however, shows $[Al_3]$ triangles that are surrounded by hexagons of Ni atoms in the $ab$-plane as well as form the triangular faces of the trigonal prisms surrounding the other Ni atoms along the $c$ direction. $CeNi_4Al$ is built up from chains and layers of vertex-sharing trigonal bipyramids with Al atoms occupying sites in the equatorial planes of these bipyramids.

Most of the compounds in the Ce–Ni–Al system show similar physical behavior. The major differences among all these compounds are the temperatures where the phenomena occur and their magnitude. For example, in
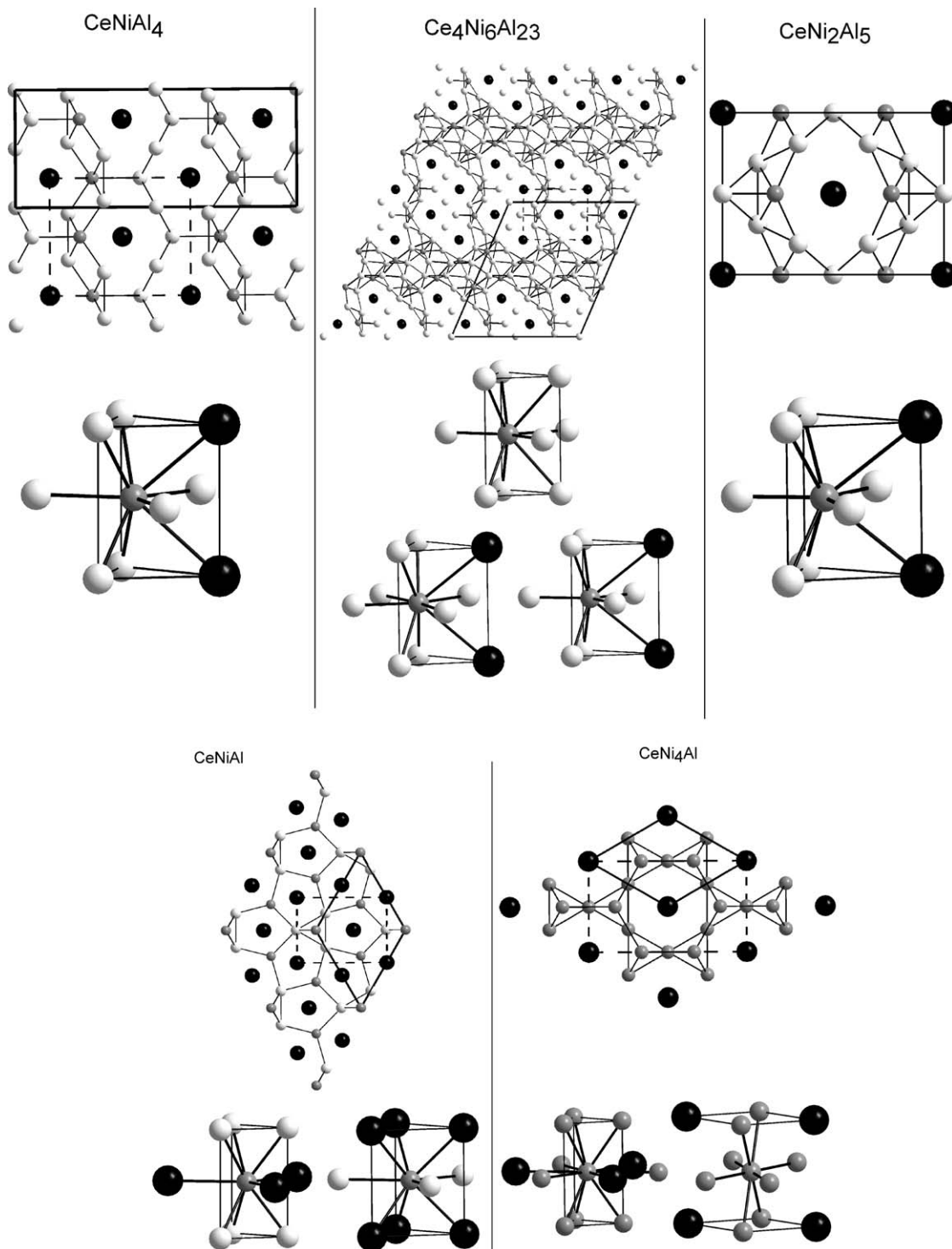
Fig. 2. Atomic arrangements observed in CeNiAl$_4$ (YNiAl$_4$-type), Ce$_4$Ni$_6$Al$_{23}$ and CeNi$_2$Al$_5$ (PrNi$_2$Al$_5$-type), CeNiAl (Fe$_2$P-type) and CeNi$_4$Al (CaCu$_5$-type). The unit cell of each compound is shown and below are presented the local environments of Ni atoms. Emphasized by dashed lines we identify a subcell close to the orthorhombic unit cell of CeNi$_2$Al$_5$. Gray, black and white circles represents Ni, Ce and Al, respectively.

Fig. 3, we show the temperature dependences of the resistance, $R$, susceptibility $\chi$ and specific heat for Ce$_4$Ni$_6$Al$_{23}$, a new structure type recently refined in the Ce–Ni–Al system, which possesses typical properties [12]. Deviations in the resistance and susceptibility begin

to occur around 100 K, which corresponds to the so-called Kondo temperature where the phenomenon of electron correlation is noticeable. Above 100 K, the susceptibility follows the Curie–Weiss law with effective moment $\mu_{eff} = 2.60\mu_B$, which is close to the free Ce$^{3+}$
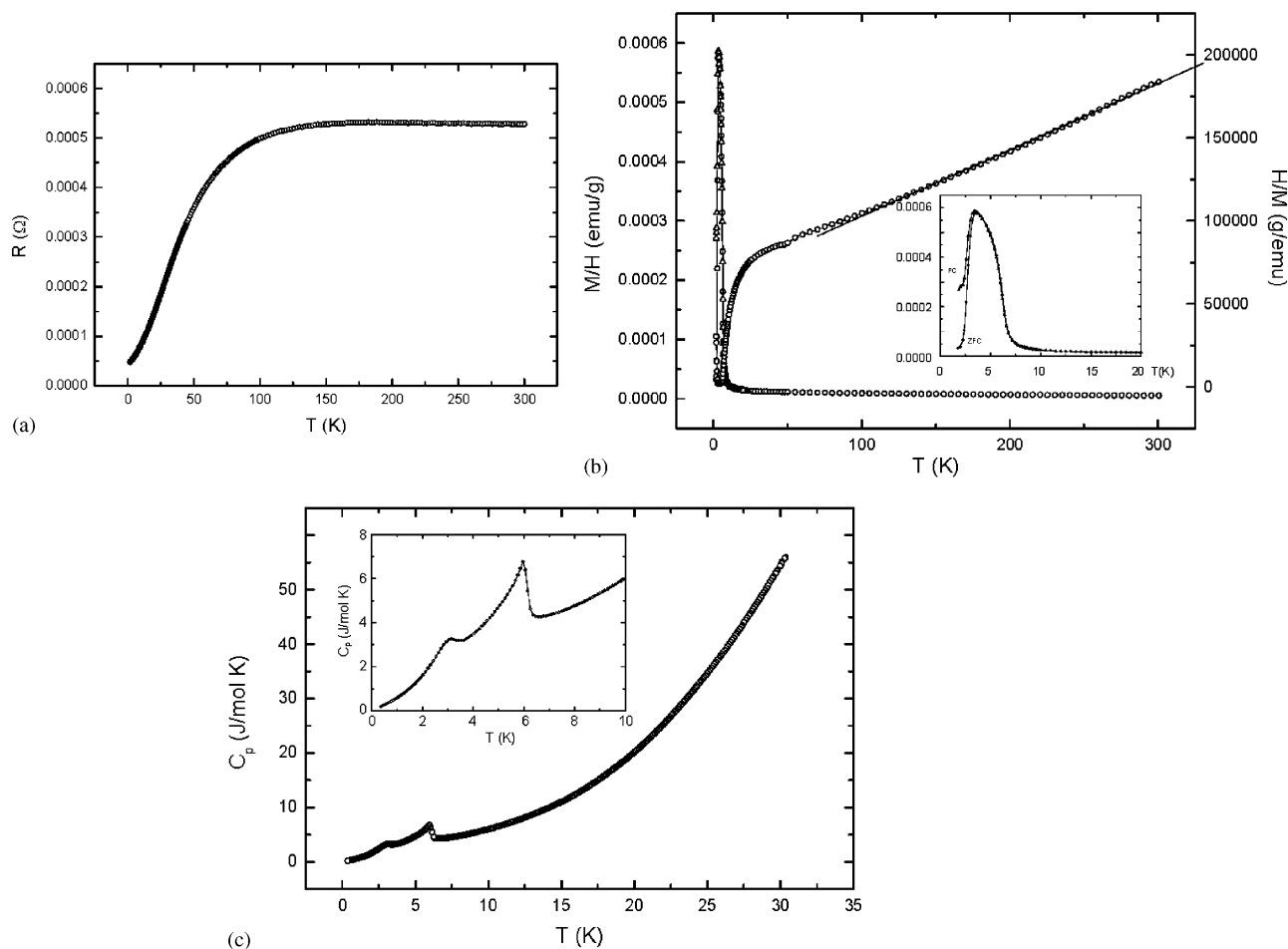
Fig. 3. Temperature dependence of (a) the resistance, (b) the susceptibility $\chi$ and the reciprocal susceptibility $1/\chi$ between 0 and 300 K and (c) of the entropy S between 0 and 35 K of a bulk of $Ce_4Ni_6Al_{23}$ sample.

ion value of $2.54\mu_B$. The Ce ions of this compound above 100 K are in a trivalent state as observed for $CeNiAl_4$, considering that the Ni ions do not contribute to the effective moment. Below 100 K, the reciprocal susceptibility $1/\chi$ slightly increases then rapidly decreases and deviates from the Curie–Weiss law. The paramagnetic Curie temperature extrapolated for $Ce_4Ni_6Al_{23}$ from the high temperature data is $\theta_p = -225$ K. This large negative paramagnetic Curie temperature is in good agreement with strong electronic correlations. The specific heat measurement is also characteristic with the presence of two anomalies at very low temperature (3 and 6 K). These anomalies were already suspected from the susceptibility measurements. Mizushima et al. also observed an anomaly in this temperature range for $CeNiAl_4$, which was explained by a valence fluctuation for $CeNiAl_4$. Table 1 summarizes the principal values (paramagnetic Curie temperature, Kondo temperature, and $\gamma_0$) for various Ce–Ni–Al compounds, which characterize the nature of these electron interactions. The CeNiAl $\gamma_0$ value is relatively low for a mixed-valence compound compared to the

Table 1
Physical and computational data on $CeNiAl_4$, $Ce_4Ni_6Al_{23}$, $CeNi_2Al_5$, and CeNiAl

| Compound | $CeNiAl_4$ | $Ce_4Ni_6Al_{23}$ | $CeNi_2Al_5$ | CeNiAl |
|---|---|---|---|---|
| $\theta_p$(K) | −200 | −225 | −196 | — |
| $\gamma_0$(mJ/mol K$^2$) | 175 | 130 | 165 | 72.5 |
| $T_{Kondo}$(K) | 120 | 100–120 | 120 | 100 |
| $N(E_F)$ (states/eV/Ce) | 3.5 | 4.3 | 3.0 | 1.0 |
| $R_{WS}$ (Ce) (Å) | 1.829 | 1.986/1.978 | 1.903 | 1.808 |
| $R_{WS}$ (Ni) (Å) | 1.386 | 1.343/1.379 | 1.320 | 1.330 |
| $R_{WS}$ (Al) (Å) | 1.387–1.470 | 1.254–1.406 | 1.323–1.387 | 1.48 |
| $R_{ES}$ (Å) | 0.560–0.729 | — | 0.549–1.012 | 0.587–0.712 |

others listed, which has been attributed to stronger hybridization of Ce-4f orbitals with Ni-3d and Al-3p orbitals and consequent 4f electron delocalization and presence of 4f states at the Fermi level. In fact, the measurement of $\gamma$ provides direct information about $N(E_F)$, the number of states at the Fermi level [17]. Indeed, the coefficient of the specific heat $C_{eletronic}$ is linear in $T$ ($C_{eletronic} = \gamma T$). On the other hand, if we

differentiate the energy with respect to temperature we obtain that: $C_{\text{eletronic}} = 1/3\pi^2 k^2 TN(E_F)$. These two last equations imply the relation: $\gamma = 1/3\pi^2 k^2 N(E_F)$. We refer the reader to the series of papers by Isikawa et al. [6–8] and Kashiwakura et al. [10] for further data and explanation about the physical measurements for such compounds in the Ce–Ni–Al systems.

## 3. Electronic structure calculations

TB-LMTO electronic band structure calculations were carried out on $Ce_4Ni_6Al_{23}$, $CeNiAl_4$, $CeNi_2Al_5$, CeNiAl and $CeNi_4Al$ in the atomic sphere approximation using the LMTO47 program [18]. Exchange and correlation were treated in a local spin density approximation [19]. All relativistic effects except spin–orbit coupling were taken into account using a scalar relativistic approximation [20].

In the atomic sphere approximation, space is filled with small overlapping Wigner–Seitz (WS) atomic spheres. The symmetry of the potential is considered to be spherical inside each WS sphere, and a combined correction takes into account the overlapping part [21]. The radii of the WS spheres were obtained by requiring that the overlapping potential be the best possible approximation to the full potential, and were determined by an automatic procedure [21]. This overlap should not be too large because the error in the kinetic energy introduced by the combined correction is proportional to the fourth power of the relative sphere overlap. Interstitial spheres are needed because the structures of the compounds under examination are not densely packed. The optimal positions and radii ($R_{\text{ES}}$) of these "empty spheres" (ES) are specified in the Table 1.

The basis set included Al 3s, 3p and 3d orbitals, Ce 6s, 6p, 5d and 4f orbitals and Ni 4s, 4p and 3d orbitals. For the ES, s and p orbitals or s, p and d orbitals were used depending on the size of the sphere. The Al 3d, Ce 6p and the ES p and d orbitals were treated by the Löwdin downfolding technique [18]. The **k**-space integrations were performed by the tetrahedron method [22]. The self-consistent charge density was obtained using 32 irreducible **k**-points in the Brillouin zone for $Ce_4Ni_6Al_{23}$, 56 for $CeNi_4Al$ and for $CeNiAl_4$, 46 for $Ce_4Ni_6Al_{23}$, 75 for CeNiAl. The contribution of the nonspherical part of the charge density to the potential was neglected.

## 4. Results and discussion

### 4.1. CeNiAl₄, Ce₄Ni₆Al₂₃, CeNi₂Al₅ and CeNiAl

We have recently investigated the electronic structure of $CeNiAl_4$ and $Ce_4Ni_6Al_{23}$ [12]. These two compounds are very close in composition ($Ce_{0.17}Ni_{0.17}Al_{0.66}$ and $Ce_{0.12}Ni_{0.18}Al_{0.70}$) and also in the local environment of the Ce atoms, which contribute to similar physical properties. To continue this study we have also calculated the electronic structures of $CeNi_2Al_5$ and CeNiAl. Indeed, $CeNiAl_4$ and $CeNi_2Al_5$ are the two most studied compounds in the Ce–Ni–Al system [8,10]. X-ray spectra obtained by X-ray photoelectron spectroscopy (XPS) show similar features in the electronic structures around the corresponding Fermi levels for these two compounds [10]. The Ni-3d bands lie ca. 2 eV below the Fermi level, which is consistent with a Ni-$d^{10}$ configuration, and some contributions from the Ce-4f orbitals are observed at the Fermi level.

In Fig. 4 the calculated total densities of states (TDOS) and the partial densities of states (PDOS) from Ni and Al are shown for $CeNiAl_4$, $Ce_4Ni_6Al_{23}$, $CeNi_2Al_5$ and CeNiAl with the energy reference as the corresponding Fermi levels. In all cases, the Fermi level falls near a minimum in the Ni and Al PDOS. Between $-4$ and $-1$ eV, the DOS are mostly from Ni-3d and Al-3p orbitals with the strong peak just below $-2$ eV due to Ni-3d orbitals. The exact position and dispersion of these orbitals depends on the composition: for the three Al-rich compounds, this band is centered at 2.5 eV below the Fermi level, while it is 2.3 eV below the Fermi level in CeNiAl. Just above the Fermi level in all examples, a large peak from the Ce-4f orbitals occurs, then the Ce-5d orbitals appear about 1 eV above the Fermi level. The large peak assigned to Ce-4f orbitals also contains contributions from Al-3p and Ni-3d levels, which suggests interactions between these orbitals of the conduction band and the Ce-4f orbitals. This is unusual considering that Ce-4f orbitals are not often considered as involved in chemical bonding, but as localized states. Moreover, integrating the Ce-4f PDOS indicates a small Ce-4f contribution to the occupied states of these compounds. Finally, integrating the unoccupied Ni-3d and Al-3p states in the Ce-4f energy region just above the Fermi level confirms that interactions between valence orbitals and Ce-4f orbitals are slightly stronger in CeNiAl since we have 5–7% more of these unoccupied states than for the Al-rich compounds. These observations are in agreement with the previous hypothesis and may explain the low $\gamma_0$ value for CeNiAl. Otherwise, since the $\gamma_0$ value is an indicator of the number of states at the Fermi level, the Fermi level for CeNiAl should be in a lower region of the DOS than for the other, more Al-rich compounds. This is observed in Fig. 4 and seen in the list of DOS values at the Fermi level for these compounds in Table 2. These calculations confirm the existence of interactions between the valence band with Ce-4f orbitals.

Furthermore, these DOS indicate an electronic configuration close to Ni $- 3d^{10}$ in these compounds. Since there is a pseudo-gap in the Ni and Al PDOS curves
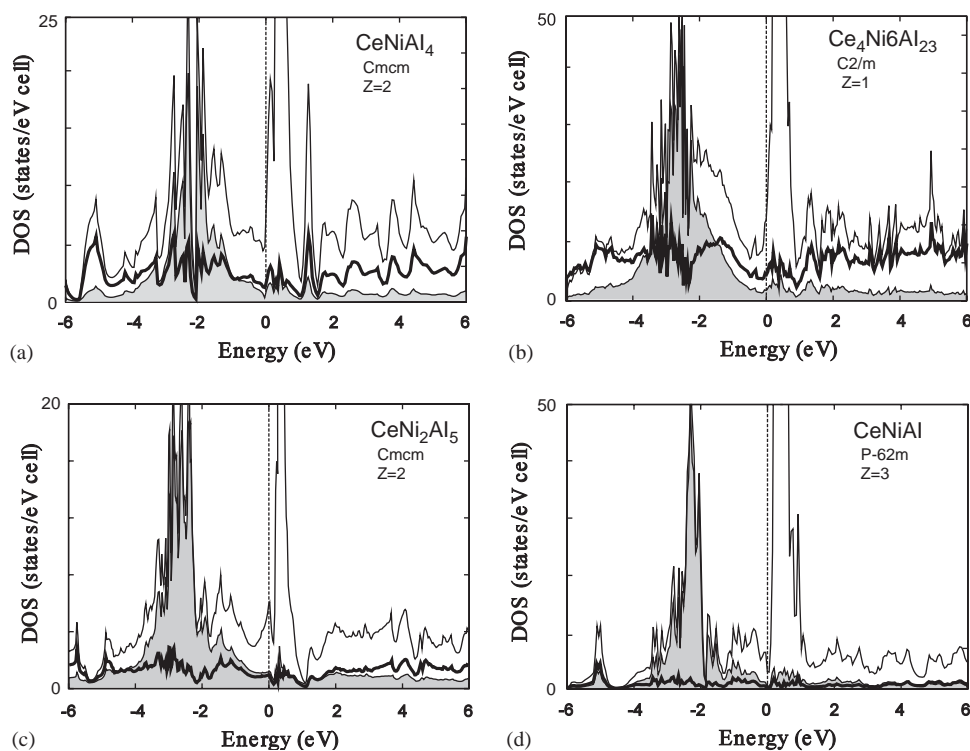
Fig. 4. TDOS, Ni PDOS and Al PDOS for (a) CeNiAl$_4$, (b) Ce$_4$Ni$_6$Al$_{23}$, (c) CeNi$_2$Al$_5$ and (d) CeNiAl. The Ni PDOS are filled in gray and the Al PDOS are delimited by a thicker line than the TDOS.

Table 2
Center of gravity values (eV) relative to the Fermi levels for valence bands at Ni sites in Ce–Ni–Al systems

|  | CeNiAl$_4$ | Ce$_4$Ni$_6$Al$_{23}$ | | | CeNi$_2$Al$_5$ | CeNiAl | | CeNi$_4$Al | |
| --- | --- | --- | --- | --- | --- | --- | --- | --- | --- |
|  | Ni | Ni$_1$ | Ni$_2$ | Ni$_3$ | Ni | Ni$_1$ | Ni$_2$ | Ni$_1$ | Ni$_2$ |
| 3d | −1.91 | −2.14 | −2.03 | −1.99 | −2.12 | −2.04 | −1.98 | −1.66 | −1.58 |
| 4s | −4.04 | −4.22 | −4.32 | −4.08 | −4.10 | −4.34 | −4.52 | −3.71 | −3.54 |

near the Fermi levels, these structures may be strongly influenced by the concentration (number) of valence electrons. For example, in CeNiAl, let us concentrate on the [Al$_3$] triangles: since each Al is two-bonded to other Al atoms, then according to the Zintl–Klemm formalism [23], the triangle requires 18 valence electrons (9 valence orbitals). Therefore, in the unit cell of CeNiAl, we anticipate an optimal valence electron count of 48 valence electrons (18 from [Al$_3$] and 30 from 3 Ni-3$d^{10}$ atoms). Note that CeNiAl shows 48–51 valence electrons if Ce donates 3–4 valence electrons to the Ni–Al framework. Of course, this simple analysis does not take into account orbital interactions between Ce and Ni or Ce and Al, which may be termed "lattice covalency" [24]. For the Al-rich examples, such an electron counting scheme is more challenging because the local coordination at each Al atom by other Al atoms does not resemble typical coordination environments for main

group elements (i.e., tetrahedral, trigonal pyramidal, etc.) Nevertheless, optimal valence electron configurations for Al–Al bonding can be estimated through Extended Hückel (EHT) calculations on just the Al networks in these structures [25][1] by determining the valence electron count that maximizes Al–Al overlap populations. The assumption in this analysis is that the Ni-4$s$ orbital will affect the dispersion of the Al valence 3$s$ and 3$p$ bands, but not their relative positions in the DOS. Furthermore, as seen in the TB-LMTO-ASA calculations, the Ni-3$d$ band is filled, well below the Fermi level, and only slightly affects the Al DOS.

---

[1] EHT calculations carried out on the Al networks for CeNiAl$_4$, Ce$_4$Ni$_6$Al$_{23}$ and CeNi$_2$Al$_5$: Al atomic orbital parameters are 3$s$ ($\zeta = 1.37, H_{ii} = -12.3$ eV) and 3$p$ ($\zeta = 1.36, H_{ii} = -6.5$ eV); 500 special k-points within the irreducible wedges of the first Brillouin zones; overlaps included for second nearest-neighbor interactions.

According to these semi-empirical calculations, we achieve the following optimal valence electron counts for Al–Al bonding (in valence electrons per formula unit): for $CeNiAl_4$, 14-15e$^-$; for $CeNi_2Al_5$, 17-18e$^-$; and for $Ce_4Ni_6Al_{23}$, 80-84e$^-$. If we now include the $Ni-3d^{10}$ valence electrons, the optimal valence electron counts are: for $CeNiAl_4$, 24-25e$^-$ (observed, 25-26e$^-$); for $CeNi_2Al_5$, 37-38e$^-$ (observed, 38-39e$^-$); and for $Ce_4Ni_6Al_{23}$, 140-144e$^-$ (observed, 141-145e$^-$).

To specifically analyze the different interatomic orbital interactions in $CeNiAl_4$, $CeNi_2Al_5$, $Ce_4Ni_6Al_{23}$ and CeNiAl, various COHPs [26] have been examined for the interatomic distances within the first coordination spheres for all atoms in these structures. These COHP curves show similar characteristics for all Al-rich compounds and only those for $CeNiAl_4$ and CeNiAl are illustrated in Figs. 5 and 6. The curves in Fig. 5 are for Ni–Al and Al–Al interactions, while Fig. 6 highlights Ce–Ni and Ce–Al. The –COHP values for Ni–Ni interactions are essentially zero because the Ni–Ni distances exceed 4 Å. –COHPs of the Al–Ni, Ce–Ni and Al–Al interactions show a crossing point between orbitals bonding and antibonding levels near the Fermi level. Indeed, most of the bonding orbitals are populated whereas antibonding orbitals remain empty. For the Al-rich examples, these crossings are especially prominent for the Al–Al orbital interactions; above the Fermi level the Ni–Al orbital interactions show either antibonding or nonbonding character. These COHP results are consistent with recent investigations of "polar intermetallics" [13,14], and demonstrate that in the Ce–Ni–Al system, different structures may arise that will optimize bonding within the electronegative Ni–Al component. In CeNiAl, the Ni–Al and Al–Al orbital interactions are nearly optimized (the corresponding integrated –COHP values are minimized), which is in accord with the low DOS value at the Fermi level and the electron counting scheme above. However, CeNiAl differs from the Al-rich examples in Ce–Ni and Ce–Al COHP curves: Ce–Ni and Ce–Al interactions are optimized (or very nearly so) in the Al-rich examples, but not in CeNiAl. Above the Fermi level in CeNiAl, there remain weakly bonding Ce–Ni and Ce–Al levels. Thus, subtle changes in the local electronic configuration at Ce can disrupt Ce–Ni and Ce–Al orbital interactions in the Al-rich examples, but should show minimal effects in CeNiAl. In this way, we may anticipate interesting physical behavior for Ce-containing intermetallic compounds that also show "polar intermetallic" characteristics with additional optimized "lattice covalency." Lattice covalency was invoked by Corbett et al. to understand the stability of $Ln_3Tt_5$
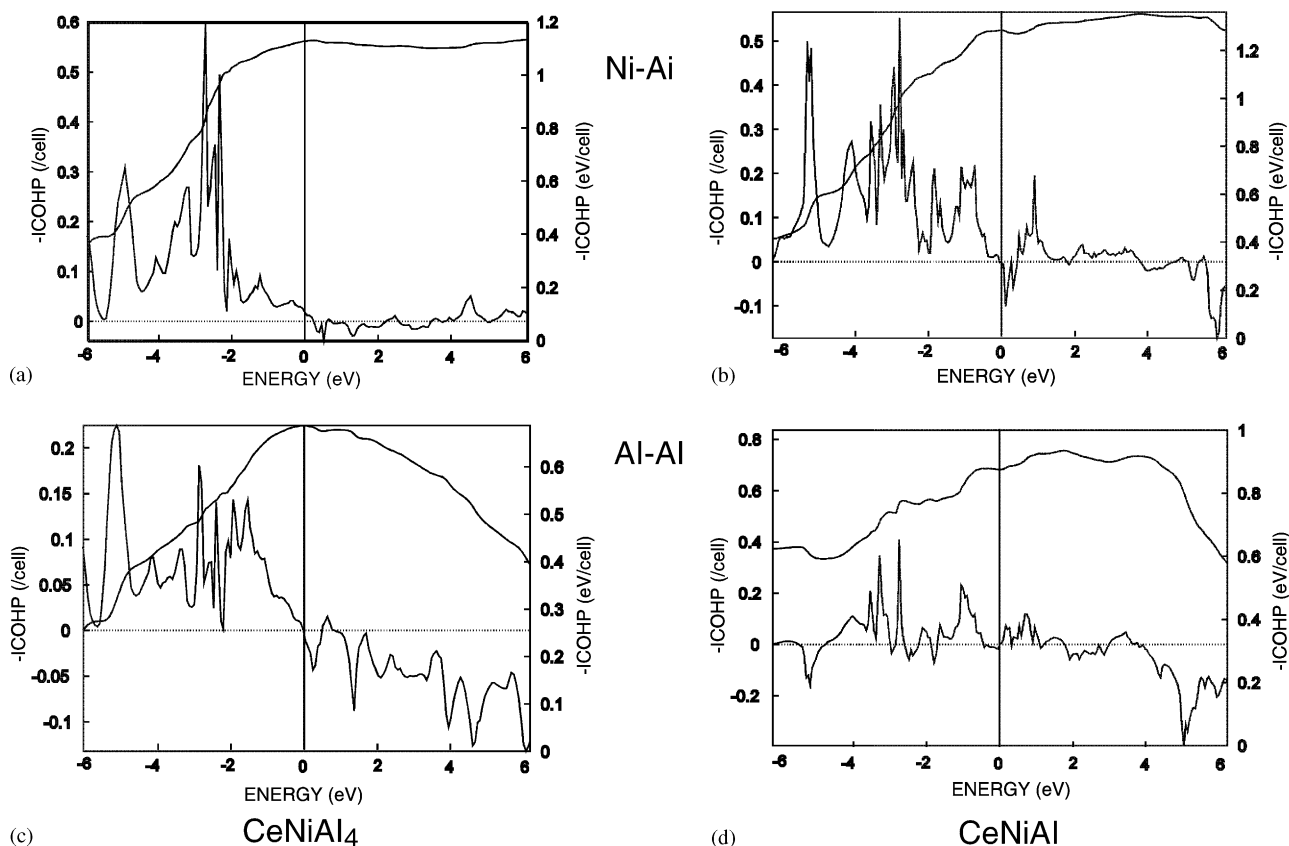


Fig. 5. COHP and integrated COHP (ICOHP) in $CeNiAl_4$ and CeNiAl for (a,b) Al–Ni and (c,d) Al–Al short distances interactions.
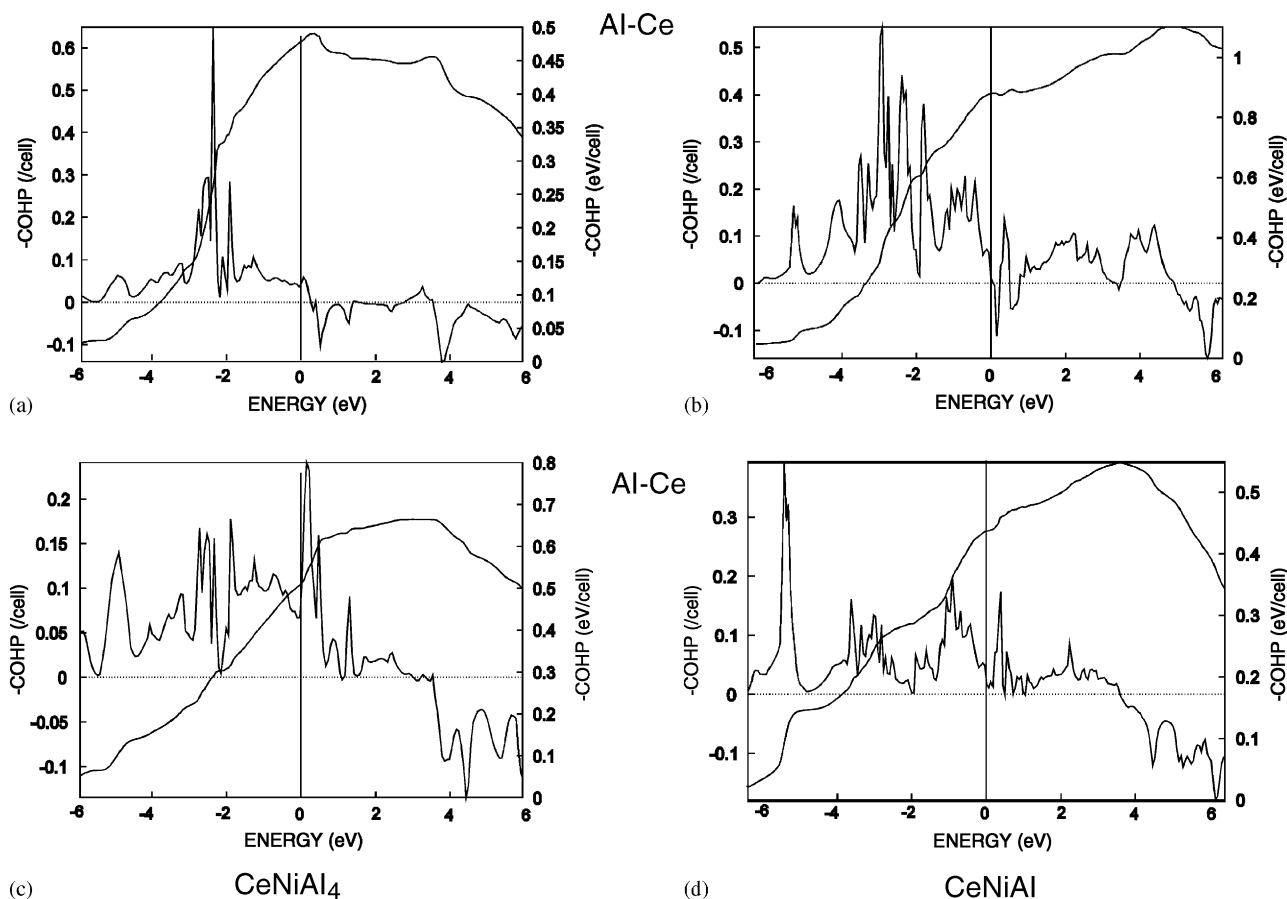
Fig. 6. COHP and integrated COHP (ICOHP) in CeNiAl$_4$ and CeNiAl for (a,b) Ce–Ni and (c,d) Ce–Al short distances interactions.

($Ln$ = rare earth element; $Tt$ = In, Sn and Pb)—Ln–Tt orbital interactions become significant around the Fermi level and contribute to chemical bonding factors that influence structure.

While DOS and COHP analysis hints at the possible interactions between the valence band and the Ce-4$f$ orbitals, band structure analysis and electron density maps provide more details into the nature of these interactions. The band structure of CeNiAl$_4$ is shown in Fig. 7 using a "fatband" representation for the Ce-4$f$ orbitals (the amount of Ce-4$f$ character in the band is represented by the width of the band). At some **k**-points we can see stabilization and destabilization of some bands with Ce-4$f$ character by as much as 1.5 eV relative to the 4$f$ band center. Electron density calculations have been performed for three special **k**-points ($\Gamma$, $Z$ and $Y$) on small energy windows including one or two bands for each point. The three plots presented in Fig. 7 show bonding interactions between Ce-4$f$ orbitals with other Ce-4$f$ orbitals as well as with Ni-3$d$ and Al-3$p$ orbitals. In the center of the square, which represents the $(a, b)$ plane at $z = \frac{1}{4}$, we recognize the shape of some Ce-4$f$ orbitals. These three plots show only bonding interactions, which stabilize these bands.

However, there are also orbitals in the conduction band that correspond to the antibonding cases. Moreover, only interactions in the $(a, b)$ plane are shown in these plots, whereas the study of other bands for other energy windows and other **k**-points identifies interactions in the $c$ direction also.

Fig. 8 shows the band structure of CeNiAl to confirm the difference in the interactions between the valence band and the Ce-4$f$ bands with those in CeNiAl$_4$ (Fig. 7). The "fatbands" indicate the Ce-4$f$ contributions of each band. By comparing the band structures of CeNiAl$_4$ (Fig. 7) and CeNiAl (Fig. 8), we confirm stronger interactions between the valence band and the Ce-4$f$ bands in CeNiAl since the dispersion of Ce-4$f$ bands is ca. 2 eV in CeNiAl, but only ca. 1 eV in CeNiAl$_4$. As one example of these interactions, an electron density map in the $(a, c)$ plane for the lowest energy Ce-4$f$ orbital at the $\Gamma$-point of CeNiAl is also shown.

### 4.2. CeNi$_4$Al

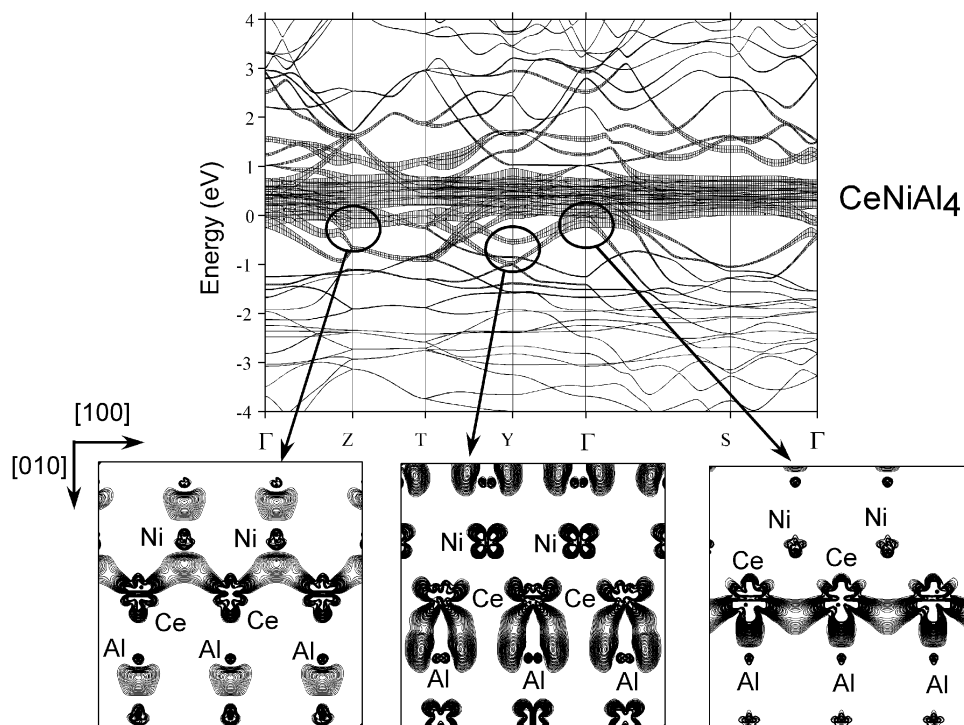In the CaCu$_5$ structure type ($P6/mmm$ symmetry) of CeNi$_4$Al, there are two possible "ordered" substitution

Fig. 7. Energy band dispersion of CeNiAl$_4$ with a fatband contribution for Ce-4$f$. $\Gamma = (0,0,0)$, $Z = (0,0,1/2)$, $T = (0,1/2,1/2)$, $Y = (0,1/2,0)$, and $S = (1/2,1/2,0)$. Below, three electron density maps for some specials energies and special **k**-points (circles) are shown. These maps correspond to the $(a,b)$ plane at $z = 1/4$.

patterns for the Al atoms to replace Ni atoms: at the crystallographic $2c$ or $3g$ sites. In carrying out TB-LMTO-ASA calculations for these two possibilities, two ordered arrangements were examined: (i) $P3$ symmetry with Al in one of the $2c$ sites; and (ii) $Cmmm$ symmetry with Al in one of the $3g$ sites and no short Al–Al contacts. For the calculations on these two models, the numbers of empty spheres and all Wigner–Seitz radii were set equal from one model to the other. The calculated total electronic energies confirm the observation of Moze and Buschow [16] since the second model, in which the Al atoms exclusively occupy the $3g$ sites, is 0.5 eV/formula unit lower than the first model. Further details concerning the structural models for the calculations are available from the authors. Fig. 9 illustrates the DOS, the Ni–Ni COHP and the Al–Ni COHP for the lower-energy model of CeNi$_4$Al. The TDOS is comparable to those for the other Ce–Ni–Al compounds (Fig. 4), but the Ni-3$d$ block is significantly broader, which suggests Ni–Ni interactions. These interactions are confirmed by the Ni–Ni COHP analysis. More Ni-3$d$ states appear just above the Fermi level than in the other Ce–Ni–Al compounds. Indeed, integration of these Ni-3$d$ states shows close to 0.5 more unoccupied state in this energy region. According to this analysis, CeNi$_4$Al does not show definitive characteristics of "polar intermetallic" compounds since bonding Ni–Ni

and Al–Ni orbital interactions remain above the Fermi level. Furthermore, the DOS value at the Fermi level is highest among the five examples we have examined (see Table 1), and arises from significant contributions from Ni-3$d$ states.

Finally, we notice that the energy centers of gravity of the Ni-3$d$ and 4$s$ bands vary among the different compounds and critically depend on their coordination environments (see Table 2). Among the Al-rich examples, the centers of the Ni-3$d$ orbitals range from 1.91 to 2.12 eV below the Fermi level as the Ni:Ce ratio increases. In CeNiAl, this center lies 2.00 below the Fermi level, whereas it is just 1.60 eV below the Fermi level in the Ni-rich example, CeNi$_4$Al. In addition, the Ni-4$s$ band center lies highest for CeNi$_4$Al and lowest for CeNiAl, which indicates a greater contribution from Ni-4$s$ orbitals to the chemical bonding in CeNiAl. Finally, the different Ni environments are readily apparent from the values for Ce$_4$Ni$_6$Al$_{23}$: one Ni site (Ni2) closely resembles the Ni1 site in CeNiAl and another site (Ni3) is similar to the Ni site in CeNiAl$_4$. The differences in these band center values originate from both the coordination environment as well as the valence electron concentration building up at these sites. In CeNi$_4$Al, the Ni atoms show a more reduced state than in the Al-rich examples.
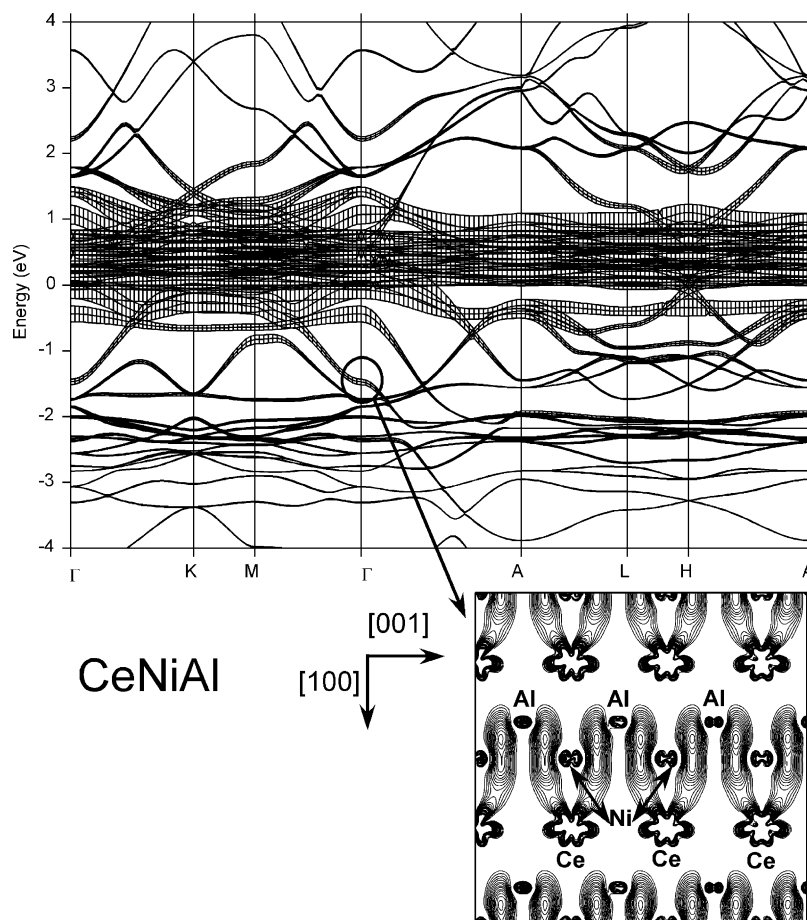
Fig. 8. Energy band dispersion of CeNiAl with a fatband contribution for Ce-4$f$. $\Gamma = (0, 0, 0)$, $K = (0, 1/2, 0)$, $M = (1/2, 1/2, 0)$, $A = (0, 0, 1/2)$, $L = (1/2, 1/2, 1/2)$ and $H = (0, 1/2, 1/2)$. Below, an electron density map at $\Gamma$-point for the most stable band with Ce-4$f$ character is shown.

## 5. Summary

Analysis of the electronic structure and chemical bonding in $Ce_4Ni_6Al_{23}$, $CeNiAl_4$, $CeNi_2Al_5$ and CeNiAl shows the "polar intermetallic" character of the Ni–Al network. On the other hand, the electronic structure of $CeNi_4Al$ differs since Ni–Ni antibonding interactions appear at the Fermi level. At low temperature any change in the Ce valence state will affect orbital interactions in the Ni–Al net for the Al-rich compounds. Although the TB-LMTO method using the local spin density approximation does not adequately treat highly correlated systems such as heavy-fermion compounds, the computational results identifies some chemical characteristics helpful to target such behavior in other compounds. One feature is the proximity of the Ce-4$f$, Ni-3$d$ and Al-3$p$ orbital energies, which makes interactions between the Ce-4$f$ orbitals and other valence orbitals possible, in good agreement with the observed properties. Moreover, the Al-rich compounds, which show heavy-fermion behavior, demonstrate optimized Al–Al and Ni–Al bonding as well as optimized Ce–Ni interactions according to COHP analysis. CeNiAl, on the other hand, shows Ce–Ni interactions that are not optimized at the Fermi level. Furthermore, the interaction between the Ce-4$f$ orbitals and other valence orbitals in CeNiAl are stronger than in the Al-rich examples, which is consistent with physical observations. Therefore, $Ce_4Ni_6Al_{23}$, $CeNiAl_4$, $CeNi_2Al_5$ and CeNiAl may be considered as polar intermetallic compounds, while the lattice covalency associated with Ce–Ni interactions influence the physical properties. These results and conclusions suggest that there may be additional Al-rich compounds available in the Ce–Ni–Al system by varying the Ce:Ni molar ratio in which the resulting compositions and structures will optimize Al–Al and Ni–Al orbital interactions. Those compounds with significant lattice covalency involving Ce–Ni interactions may show unusual physical behavior at low temperatures. Therefore, we continue to explore new Al-rich examples in the RE–Ni–Al system.
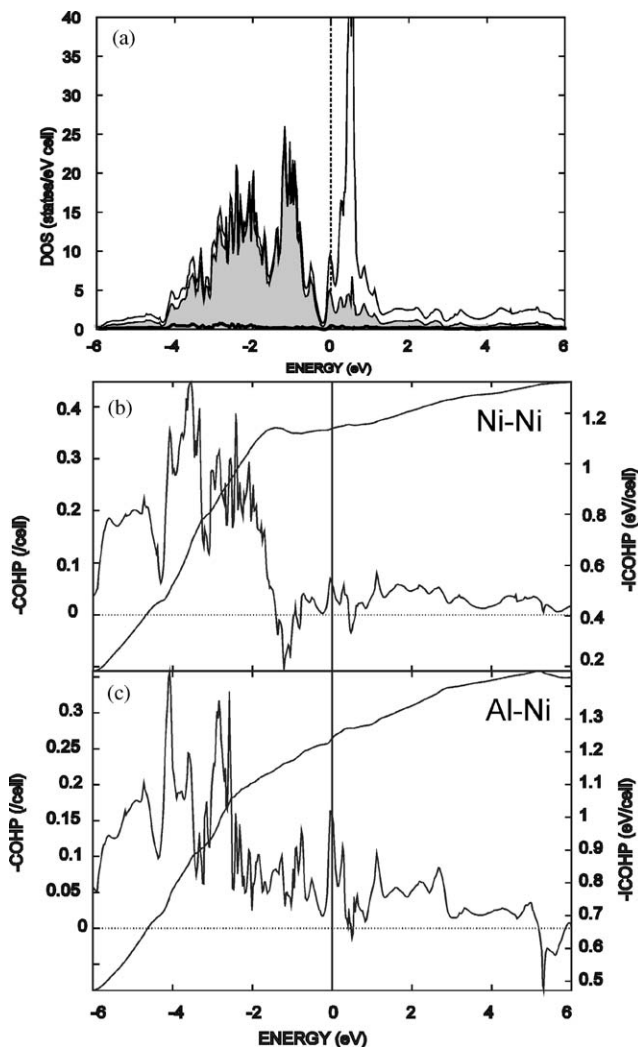
Fig. 9. (a) TDOS, Ni PDOS and Al PDOS for CeNi$_4$Al. COHP and integrated COHP (ICOHP) for (b) Ni–Ni interactions and for (c) Al–Ni interactions in CeNi$_4$Al.

## Acknowledgments

## References

[1] Z. Fisk, R.H. Ott, T.M. Rice, J.L. Smith, Science 320 (1986) 124.

[2] H. Harima, T. Kasuya, J. Magn. Magn. Mater. 52 (1985) 179.

[3] O.S. Zarechnyuk, T.I Yanson, R.M. Rykhal, Izv. Akad. Nauk SSSR Met. 4 (1983) 192.

[4] A.E. Dwight, M.H. Mueller, R.A. Conner Jr., J.W. Downey, H. Knott, Trans. Metall. Soc. AIME 242 (1968) 2075.

[5] (a) T. Mizushima, Y. Isikawa, A. Maeda, K. Oyabe, K. Mori, K. Sato, K. Kamigaki, J. Phys. Soc. Jpn. 60 (1991) 753;
(b) T. Mizushima, Y. Isikawa, K. Oyabe, K. Mori, J. Sakurai, Physica B 186 (1993) 457.

[6] Y. Isikawa, T. Mizushima, K. Oyabe, K. Mori, K. Sato, K. Kamigaki, J. Phys. Soc. Jpn. 60 (1991) 1869.

[7] Y. Isikawa, K. Mori, K. Kamigaki T. Mizushima, K. Oyabe, S. Ueda, K. Sato, J. Magn. Magn. Mater. 108 (1992) 157.

[8] Y. Isikawa, T. Mizushima, J. Sakurai, K. Mori, A. Munoz, F. Givord, J.-X. Boucherle, J. Voiron, I.S. Oliveira, J. Flouquet, J. Phys. Soc. Jpn. 63 (1994) 2349.

[9] Y. Isikawa, H. Tagaki, A. Ishugiro, M. Yasumoto, T. Kuwai, T. Mizushima, J. Sakurai, A. Sawada, T. Komatsubara, K. Maezawa, H. Harima, J. Phys. Soc. Jpn. 68 (1999) 2802.

[10] T. Kashiwakura, T. Okane, S. Suzuki, S. Sato, M. Watanabe, A. Harasawa, T. Kinoshita, A. Kakizaki, T. Ishi, S. Nakai, Y. Isikawa, J. Phys. Soc. Jpn. 69 (2000) 3095.

[11] K.M. Poduska, F.J. DiSalvo, V. Petricek, J. Alloys Compd. 308 (2000) 64.

[12] D. Gout, E. Benbow, O. Gourdon, G.J. Miller, J. Solid. State. Chem. (2003), in press.

[13] U. Häussermann, S. Amerioun, L. Eriksson, C.-S. Lee, G.J. Miller, J. Amer. Chem. Soc. 124 (2002) 4371.

[14] G.J. Miller, C.-S. Lee, W. Choe, in: G. Meyer, D. Naumann, L. Wesemann (Eds.), Inorganic Chemistry Highlights, Wiley-VCH, Berlin, 2002.

[15] D. Hall, E.C. Palm, T.P. Murphy, S.W. Tozer, C. Petrovic, E. Miller-Ricci, L. Peabody, C.Q.H. Li, U. Alver, R.G. Goodrich, J.L. Sarrao, P.G. Pagliuso, J.M. Wills, Z. Fisk, Phys. Rev. B 64 (6) (2001) 064506/1–064506/7.

[16] O. Moze, K.H.J. Buschow, J. Magn. Magn. Mater. 146 (1995) 111–116.

[17] J.M. Ziman, Principles of the Theory of Solids, Cambridge University Press, Cambridge, 1964.

[18] (a) O.K. Andersen, Phys. Rev. B 12 (1975) 3060;
(b) O.K. Andersen, O. Jepsen, Phys. Rev. Lett. 53 (1984) 2571;
(c) O.K. Andersen, O. Jepsen, D. Glötzel, in: F. Bassani, F. Fumi, M.P. Tosi (Eds.), Highlights of Condensed-Matter Theory, North-Holland, New York, 1985;
(d) O.K. Andersen, Phys. Rev. B 34 (1986) 2439.

[19] U. von Barth, L. Hedin, J. Phys. C 5 (1972) 1629.

[20] D. Koelling, B.N. Harmon, J. Phys. C 10 (1977) 3107.

[21] O. Jepsen, O.K. Andersen, Z. Phys. B 97 (1995) 645.

[22] P.E. Blöchl, O. Jepsen, O.K. Andersen, Phys. Rev. B 49 (1994) 16223.

[23] G.J. Miller, in: S.M. Kauzlarich (Ed.), Chemistry, Structure, and Bonding of Zintl Phases and Ions, VCH, New York, 1996, p. 1.

[24] M.T. Klem, J.T. Vaughey, J.G. Harp, J.D. Corbett, Inorg. Chem. 40 (2001) 7020.

[25] (a) R. Hoffmann, W.N. Lipscomb, J. Chem. Phys. 36 (1962) 2179, 3489;
(b) J.H. Ammeter, H.B. Buergi, J.C. Thibeault, R. Hoffmann, J. Am. Chem. Soc. 100 (1978) 3686;
(c) M.-H. Whangbo, R. Hoffmann, R.B. Woodward, Proc. R. Soc. London Ser. A 366 (1979) 23.

[26] R. Dronskowski, P.E. Blöchl, J. Phys. Chem. 97 (1993) 8617.